Journal of Environmental Engineering and Energy

www.jeee.reapress.com

J. Environ. Eng. Energy Vol. 3, No. 1 (2026) 1–22.

Paper Type: Original Article

Numerical Investigation of Freezing Time in Circular and Flattened Pipes Using CFD: Effects of Geometry and Flow Conditions

Hasan Asadikia[1,*], Fatemeh Aminipour[1], Asma Mozaffari[1], Zahra Khodabandeh[1], Seyed Mahmood Kia[1]

[1] Faculty of Mechanical and Energy Engineering, Shahid Beheshti University, Tehran, Iran; asadi.kia.h@gmail.com; aminipourfateme27@gmail.com; a.mozefferi@mail.sbu.ac.ir; zahra.khdbndh@gmail.com; mahmoud.kia.73@gmail.com.

Citation:

Received: 19 May 2025 *Revised: 1 August 2025* *Accepted: 12 September 2025*	Asadikia, H., Aminipour, F., Mozaffari, A., Khodabandeh, Z., & Kia, S. M. (2026). Numerical investigation of freezing time in circular and flattened pipes using CFD: Effects of geometry and flow conditions. *Journal of Environmental Engineering and Energy*, *3*(1), 1-22.

Abstract

This study presents a computational investigation of the freezing process in circular and geometrically deformed (flattened) pipes using Computational Fluid Dynamics (CFD). The objective is to evaluate the impact of pipe geometry and flow conditions on freezing time and ice plug formation. A series of CFD simulations was conducted on pipes ranging from 1 to 5 inches in diameter, under both stationary and flowing fluid conditions, with varying degrees of flattening (0%–25%) and flow velocities within the laminar regime. The governing equations of mass, momentum, and energy conservation were applied in both Cartesian and cylindrical coordinates. Results indicate that pipe flattening significantly reduces freezing time, especially in larger diameters, due to increased heat transfer efficiency. Additionally, fluid velocity was found to delay freezing, with the effect more pronounced in wider pipes. Simulation outputs, including thermal profiles and freezing fronts, validated these findings. The results provide valuable insights for optimizing pipeline maintenance operations using cryogenic freezing techniques, enabling fluid isolation without full drainage or shutdown.

Keywords: Computational fluid dynamics, Pipe freezing, Ice plug, Deformation, Heat transfer, cryogenic.

1 | Introduction

Fluid transmission pipelines constitute a critical component of the operations of numerous industries, such as oil and gas, petrochemicals, thermal power generation, and utility services. Such pipelines are, however, prone to risks such as corrosion, cracking, and mechanical failure that require regular maintenance and repair activities. Preventing fluid leakage and reducing losses during repair activities is one of the biggest concerns relating to pipeline maintenance because these can cause expensive operating costs and even environmental

Corresponding Author: asadi.kia.h@gmail.com
https://doi.org/10.22105/jeee.v3i1.59

issues. Various techniques can be employed in pipeline repair, with each one of them carrying some merits and demerits.

A few of the techniques utilized in pipeline repair are cutting and draining, pigging, and freezing techniques. Cutting and draining entails cutting out a section of pipe, necessitating a complete halt in fluid flow; however, this technique leads to fluid loss, increased expense, and potential environmental damage. The pigging technique involves using a mechanical device that travels through the pipe to break or clean the fluid first before repairs are carried out. Still, it requires specialized equipment that may not apply in all circumstances. The freezing technique offers a more effective alternative by allowing repairs without the fluid's complete draining.

In the freezing technique, a cryogenic refrigerant, i.e., liquid nitrogen, is employed to freeze a portion of the fluid, which is in the pipe, to form an ice plug that temporarily impedes flow. This is commonly utilized due to simplicity, low expense, and less environmental impact. However, its behavior is influenced by a number of parameters, including pipe diameter, initial temperature of the fluid, flow pressure, rate of heat transfer, and pipe geometry. Any alteration in pipeline geometry, particularly in deformed (collapsed) pipe, has the inclination to alter heat transfer rates and significantly influence freezing time.

Heat transfer is an essential factor in pipeline freezing and can influence ice plug formation, stability, and efficiency [1–3]. The involved process relies on conduction, convection, and phase change, while pipe diameter, fluid temperature, fluid velocity, and geometry affect freezing time. Deformed pipes lead to non-uniform heat transfer behavior, which further influences the system's freezing competence and structural integrity. Knowledge of these effects is important to optimize the freezing method and minimize downtime. In this study, Computational Fluid Dynamics (CFD) simulations are used to investigate the freezing of circular and noncircular pipes, focusing on the effect of geometry and flow conditions on heat transfer and ice plug at the inlet of the pipe [4], [5].

Freezing operation success depends primarily on the phenomena of heat conduction and the prevailing modes of fluid flow within the pipe. Understanding the thermal behavior of the ice plug and that of the surrounding fluid is the cornerstone of estimating the frozen seal integrity and freezing time. Heat conduction, convection, and phase change create a balance that is accountable for the ice plug formation mode and rate [6–10].

Many studies have been conducted on thermal and flow conditions with the aim of optimizing the freezing process efficiency [11–14]. In addition, the impact of the selection of parameters of the flow rate, turbulence, and temperature variation upon the formation and stability of ice plugs has been researched in the literature so far. High rates of flow can prevent freezing operations, and controlled conditions can offer efficiency. Understanding the past condition is a fundamental necessity for enhancing the techniques involved in bulk freezing of pipelines to enable the reliability of industrial processes and minimize the operational complexities in pipeline maintenance [15–18]. The present study examines the process of freezing in circular and noncircular (collapsed) pipes through the use of CFD simulations. The main aim is to examine the impact of changes in pipe geometry on heat transfer rates, freezing time, and the stability of ice plugs. Further, the research explores the effects of variations in different factors, including the initial fluid temperature and flow pressure, on the effectiveness of the freezing technique. The outcome of this study is expected to lead to an increase in the efficiency of pipeline maintenance operations and cost reduction across many industries, such as thermal power stations, oil and gas pipelines, and utility organizations.

Liu et al. [19] proposed a no-shutdown pipe repair method by applying liquid nitrogen freezing to create an ice plug, allowing maintenance to be carried out without pausing the water flow. They optimized the freezing conditions (0.7–0.8 kg/min nitrogen flow) and determined the length of the ice plug beyond the freezing jacket, confirming successful blocking. This method was effective for pipe repair in confined areas, and case studies in hospitals were undertaken to show that the method could be used successfully due to the usage of infrared imaging with ultrasonic flowmeters for procedure monitoring. Bijan Fard and Karimi [20] developed a system of pipe freezing to make a plug of ice using liquid nitrogen or CO_2, enabling maintenance procedures to be performed on pipelines without draining the fluid or turning off the entire plant. This particular method

was used to avoid the loss of fluids and prevent contamination of the fluid. It was very useful in systems having dangerous fluids like acids and highly poisonous chemicals. The study showed that pipelines could be rehabilitated through an external process as a better alternative to common drainage-based pipeline rehabilitation practices when overall economic and environmental costs were minimized, and efficiency and safety were improved. Park et al. [21] investigated the ice plugging method, where the liquid nitrogen is applied circumferentially around a pipe to freeze fluid within the pipe and then create a solid blockage that seals fluid flow. It allowed for pipeline inspection and maintenance without a full system shutdown. The study investigated the influence of different pipe geometries and freezing jacket conditions on the freezing process and heat transfer performance. Additionally, the research identified the maximum fluid flow rate at which the ice plug could form, and it was observed that for a given pipe diameter, the permissible flow rate was approximately directly proportional to the freezing jacket length. Burton [22] conducted a numerical and experimental study of ice plug formation in vertical tubes. Burton was interested in the heat and mass transfer aspects of freezing in stagnant and flowing fluids. Burton identified three phases of the ice plug formation: initial surface freezing, opposite-direction convective interactions, and ice plug growth. The results indicated that the freezing duration was highly sensitive to the pipe diameter and fluid flow rate. Tavner [23] performed an experimental freezing of vertical pipes using liquid nitrogen. The study showed that increasing the jacketed surface area under a nitrogen load had a very big impact on freezing time. Tavner modeled convective flow patterns during freezing and found two zones, one near the top of the ice plug with upward-flowing flow and one near the bottom with downward-flowing flow. The research determined the role of natural convection in heat transfer during freezing. Bowen [24] carried out experimental investigations on the morphology and development of ice plugs in pipes with varying thermal conditions. The findings indicated that the development of an ice throat was dependent on fluid temperature, pipe diameter, and flow conditions. In addition, it was observed that forced convection flows could worsen the heat transfer efficiency and increase freezing time.

2|Governing Equation

To simulate the freezing process within circular and noncircular pipes, the fundamental governing equations of fluid flow and heat transfer are applied. These include the continuity, Navier–Stokes, and energy equations, formulated under the assumptions of incompressible and Newtonian flow. The equations are expressed in both Cartesian and cylindrical coordinates to accommodate the geometry of the problem.

2.1|Continuity Equation

According to the principle of mass conservation, the net rate of mass accumulation in a control volume must be zero over time. For a fluid with density ϱ and velocity components (u, v, w), in a Cartesian coordinate system, the general form of the mass conservation equation is expressed as *Eq. (1)*.

$$\frac{\partial \mathrm{pu}}{\partial \mathrm{x}}+\frac{\partial \mathrm{pv}}{\partial \mathrm{y}}+\frac{\partial \mathrm{pw}}{\partial \mathrm{z}}+\frac{\partial \mathrm{p}}{\partial \mathrm{t}}=0. \quad \textbf{(1)}$$

For incompressible fluids, where the density is constant, *Eq. (1)* simplifies to *Eq. (2)*.

$$\frac{\partial \mathrm{u}}{\partial \mathrm{x}}+\frac{\partial \mathrm{v}}{\partial \mathrm{y}}+\frac{\partial \mathrm{w}}{\partial \mathrm{z}}\nabla.\mathrm{V}=0. \quad \textbf{(2)}$$

In this study, where fluid freezing within cylindrical pipes is analyzed, it is necessary to express the continuity equation in cylindrical coordinates. The corresponding form for incompressible flow is presented by *Eq. (3)*.

$$\frac{1}{\mathrm{r}}\frac{\partial(\mathrm{rV}_{\theta})}{\partial \mathrm{r}}+\frac{1}{\mathrm{r}}\frac{\partial \mathrm{V}_{\theta}}{\partial \theta}+\frac{\partial \mathrm{V}_{\mathrm{z}}}{\partial \mathrm{z}}=0. \quad \textbf{(3)}$$

2.2 | Navier–Stokes Equations

To analyze fluid motion and predict velocity distributions in a freezing system, the Navier–Stokes equations are employed. These equations, together with the continuity equation, form a complete and solvable system of partial differential equations for incompressible Newtonian fluids with constant density and viscosity. The momentum component in the Cartesian coordinates is given by *Eqs. (4)-(6)*.

$$\rho\left(\frac{\partial u}{\partial t}+u\frac{\partial u}{\partial x}+v\frac{\partial u}{\partial y}+w\frac{\partial u}{\partial z}\right)=\rho g_x-\frac{\partial p}{\partial x}+\mu\left(\frac{\partial^2 u}{\partial x^2}+\frac{\partial^2 u}{\partial y^2}+\frac{\partial^2 u}{\partial z^2}\right). \quad (4)$$

$$\rho\left(\frac{\partial v}{\partial t}+u\frac{\partial v}{\partial x}+v\frac{\partial v}{\partial y}+w\frac{\partial v}{\partial z}\right)=\rho g_y-\frac{\partial p}{\partial y}+\mu\left(\frac{\partial^2 v}{\partial x^2}+\frac{\partial^2 v}{\partial y^2}+\frac{\partial^2 v}{\partial z^2}\right). \quad (5)$$

$$\rho\left(\frac{\partial w}{\partial t}+u\frac{\partial w}{\partial x}+v\frac{\partial w}{\partial y}+w\frac{\partial w}{\partial z}\right)=\rho g_z-\frac{\partial p}{\partial z}+\mu\left(\frac{\partial^2 w}{\partial x^2}+\frac{\partial^2 w}{\partial y^2}+\frac{\partial^2 w}{\partial z^2}\right). \quad (6)$$

To better suit the cylindrical geometry of the problem, these equations are transformed into cylindrical coordinates, where each component (radial, azimuthal, and axial) is expressed separately, as shown in *Eqs. (7)-(9)*, respectively.

Radial component:

$$\rho\left(\frac{\partial V_r}{\partial t}+V_r\frac{\partial V_r}{\partial r}+\frac{V_\theta}{r}\frac{\partial V_r}{\partial \theta}-V_z\frac{\partial V_r}{\partial z}\right)=\rho g_r-\frac{\partial p}{\partial y}+\mu\left\{\frac{\partial}{\partial r}\left(\frac{1}{r}\frac{\partial}{\partial r}[rV_r]\right)+\frac{1}{r^2}\frac{\partial^2 V_r}{\partial \theta^2}+\frac{2}{r^2}\frac{\partial V_\theta}{\partial \theta}+\frac{\partial^2 V_r}{\partial z^2}\right\}. \quad (7)$$

Azimuthal component:

$$\rho\left(\frac{\partial V_\theta}{\partial t}+V_r\frac{\partial V_\theta}{\partial r}+\frac{V_\theta}{r}\frac{\partial V_\theta}{\partial \theta}+\frac{V_rV_\theta}{r}+V_z\frac{\partial V_\theta}{\partial z}\right)=\rho g_\theta-\frac{1}{r}\frac{\partial p}{\partial y}+\mu\left\{\frac{\partial}{\partial r}\left(\frac{1}{r}\frac{\partial}{\partial r}[rV_\theta]\right)+\frac{1}{r^2}\frac{\partial^2 V_r}{\partial \theta^2}+\frac{2}{r^2}\frac{\partial V_r}{\partial \theta}+\frac{\partial^2 V_\theta}{\partial z^2}\right\}. \quad (8)$$

Axial component:

$$\rho\left(\frac{\partial V_z}{\partial t}+V_r\frac{\partial V_z}{\partial r}+\frac{V_\theta}{r}\frac{\partial V_z}{\partial \theta}+V_z\frac{\partial V_z}{\partial z}\right)=\rho g_z-\frac{\partial p}{\partial z}+\mu\left\{\frac{1}{r}\frac{\partial}{\partial r}\left(r\frac{\partial V_z}{\partial r}\right)+\frac{1}{r^2}\frac{\partial^2 V_z}{\partial \theta^2}+\frac{\partial^2 V_z}{\partial z^2}\right\}. \quad (9)$$

2.3 | Energy Equation

In general, heat transfer occurs whenever there is a temperature gradient between two points or across a phase boundary. During the freezing process of a fluid inside a pipe, thermal energy is exchanged through both conduction and convection mechanisms. Based on the energy conservation principle, the heat flux entering the control volume equals the heat flux exiting it. Accordingly, an energy balance is required at the freezing interface between the liquid and solid phases.

This energy balance consists of three primary components: the heat required to cool the liquid from its initial temperature (TL) to the freezing temperature (Tfr), the latent heat consumed during the phase transition from liquid to solid at Tfr, and the heat conducted through the ice layer and pipe wall to the ambient environment. These steps, cooling of the liquid, phase change, and heat conduction through both solidified ice and the pipe wall, occur in sequence and are governed by the thermal properties of each layer. Additionally, the external pipe surface experiences cooling from the pipe wall temperature Ts to the ambient temperature T∞ maintained by the surrounding refrigerant (see *Fig. 1*). The total energy balance is represented in *Eq. (10)*.

$$q_1+q_2=q_3. \quad (10)$$

The overall heat flux between two regions with a temperature difference ΔT and total thermal resistance R is defined by *Eq. (11)*. The latent heat transfer during phase change is calculated using *Eq. (12)*. In contrast, the conductive and convective thermal resistances are given in *Eqs. (13)* and *(14)*, respectively.

Eq. (10) represents the general form of the energy equation, where each term is eventually expressed based on the characteristics of the pipe and the freezing fluid. Considering the temperature distribution in different regions, as shown in *Fig. 1*, the factors contributing to heat transfer include:

I. Cooling of the fluid from temperature T_L to the freezing temperature T_{fr}.

II. Phase change at the freezing temperature (transition from liquid to solid).

III. Cooling of the solid phase (reduction in the temperature of the formed ice layer).

IV. Cooling the pipe wall.

V. Cooling of the outer surface of the pipe from T_s to T_∞ (refrigerant temperature).

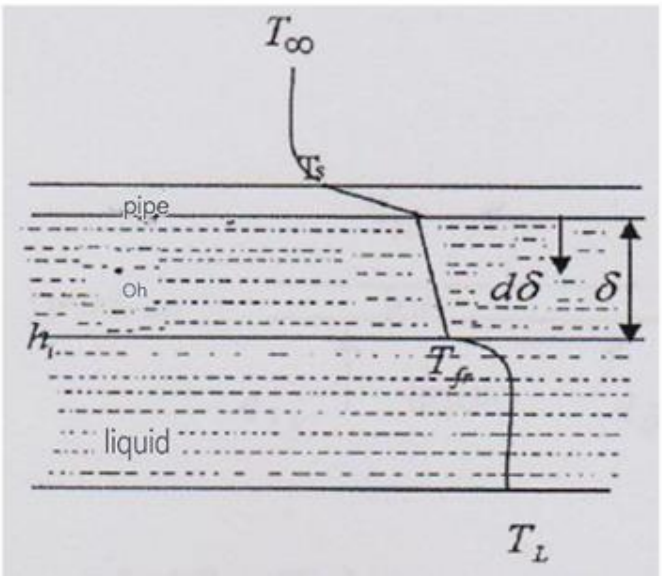

Fig. 1. Temperature changes at different points in a freezing pipe.

The heat transfer per unit time (heat flux) between two points with a temperature difference of ΔT and thermal resistance R is given by *Eq. (11)*. The heat flux due to phase change is determined by *Eq. (12)*., while the convective and conductive resistances in cylindrical coordinates are obtained from *Eqs. (13)* and *(14)*, respectively.

$$q = \frac{\Delta T}{R}. \tag{11}$$

$$q = \dot{m}L_f = \frac{d}{dt}(\rho AL)L_f\left(2\pi L(r_i - \delta)\right)\frac{d\delta}{dt}. \tag{12}$$

$$R_{cond} = \frac{In\frac{r_o}{r_i}}{2\pi KL}. \tag{13}$$

$$R_{conV} = \frac{1}{h2\pi rL}. \tag{14}$$

Due to the presence of symmetrical conditions and the effect of axial conduction, as shown in *Fig. 2*, the primary heat transfer occurs in the radial direction and towards the inside of the pipe. For this reason, the thickness of the growing ice mass forms a hollow cylinder, which increases in thickness inward over time. In other words, freezing begins from the inner surface and progresses toward the center. Therefore, to formulate the energy equation, it is sufficient to write the heat transfer equation in the radial direction.

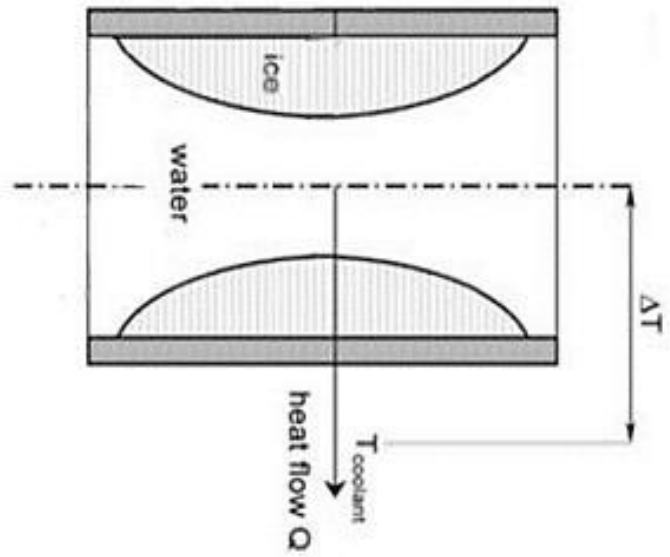

Fig. 2. Ice growth formation and direction of heat flux transfer [2].

If the convective heat transfer between the outer surface of the pipe and the surrounding environment is neglected, the outer surface temperature of the pipe can be assumed to be equal to the ambient temperature. Under these conditions, the thermal resistance in a freezing pipe will be as shown in *Fig. 3*.

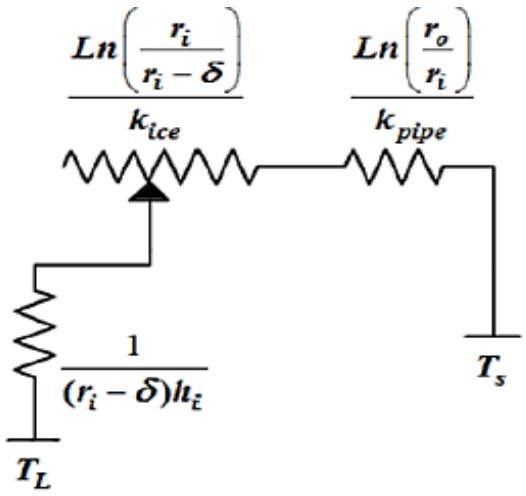

Fig. 3. Thermal resistances in a circular pipe from the fluid temperature to the outer surface temperature of the pipe [1].

Based on the provided explanations and the application of the above equations, the energy equation (*Eq. 10*) is transformed into *Eq. (15)*.

$$\frac{T_{fr}-T_s}{\frac{\ln\frac{r_i}{r_i-\delta}}{2\pi K_{ice}L}+\frac{\ln\frac{r_o}{r_i}}{2\pi K_{pipe}L}}=\frac{T_L-T_{fr}}{\frac{1}{2\pi(r_i-\delta)h_iL}}+\rho L_f\left(2\pi L(r_i-\delta)\right)\frac{d\delta}{dt}. \quad (15)$$

3 | Numerical Simulation

A numerical analysis of the freezing process in pipelines with circular and noncircular cross-sections has been conducted using the CFD approach. The primary objective of this simulation is to compare the freezing time in circular and noncircular pipes containing water, considering both stationary and flowing fluid conditions.

Fluent software, a CFD tool based on the finite volume method, has been employed in this study due to its high capability in flow analysis and its ability to solve freezing-related problems.

The Gambit software has been used as a pre-processor, while Fluent has been utilized as the solver for numerical analysis. To generate the geometric model, the complete dimensions of the pipes must first be defined. The pipes used in fluid transmission lines are typically made of carbon steel, specifically selected from the American Society for Testing and Materials (ASTM) A53 Gr. B standard. The required specifications for pipe design have been extracted from this standard and are presented in *Table 1*.

Table 1. Pipe Geometrical specifications.

Pipe Size (Inch)	Outer Diameter (mm)	Wall Thickness (mm)	Inner Diameter (mm)	Average Diameter (mm)	Unit Weight (Kg/m)	Standard Specification
1	33.4	4.55	24.3	28.85	2.44	XS
2	60.3	5.54	49.2	54.76	7.48	XS
3	88.9	5.49	77.92	83.41	11.19	STD
4	114.3	6.02	102.26	108.28	16.07	STD
5	141.3	6.55	128.2	134.75	21.72	STD

To avoid the influence of boundary conditions applied at the pipe's inlet and outlet and to minimize their impact on the simulation results, the total pipe length has been set to 120 cm. The central 30 cm of the pipe is covered by a freezing jacket, where the freezing process occurs.

For problems with symmetric geometries and boundary conditions, symmetry assumptions can be employed to reduce computational time by modeling only a portion of the domain. In circular pipes, symmetrical conditions allow for both three-dimensional and two-dimensional modeling. However, in the case of noncircular (flattened) pipes, the geometry can only be represented in three dimensions.

3.1 | Geometric Modeling

This section outlines the steps for geometric modeling of circular and noncircular pipes using Gambit software. In both cases (circular and flattened pipes), due to symmetry in the three-dimensional geometry and boundary conditions, only one-quarter of the pipe can be modeled.

The three-dimensional geometry of a symmetric circular pipe, along with the naming of different sections, is illustrated in *Fig. 4*. These labels will later be used when applying boundary conditions and during the simulation phase.

To create this geometry:

I. Two quarter-circle arcs are drawn, corresponding to the inner and outer radii of the pipe.

II. The remaining lines are added to form the pipe's cross-section, as shown in *Fig. 4*.

III. By extruding this cross-section perpendicular to the plane (along the Z-axis) by 1.3 meters, the final three-dimensional pipe geometry is generated.

To create the geometric model, two quarter-circle arcs with radii corresponding to the inner and outer surfaces of the pipe are first drawn. Then, the remaining lines are added to complete the pipe cross-section, as shown in *Fig. 5*. By extending these lines perpendicular to the plane (along the Z-axis in this case) by a length of 1.3 meters, the overall shape of the pipe is formed.

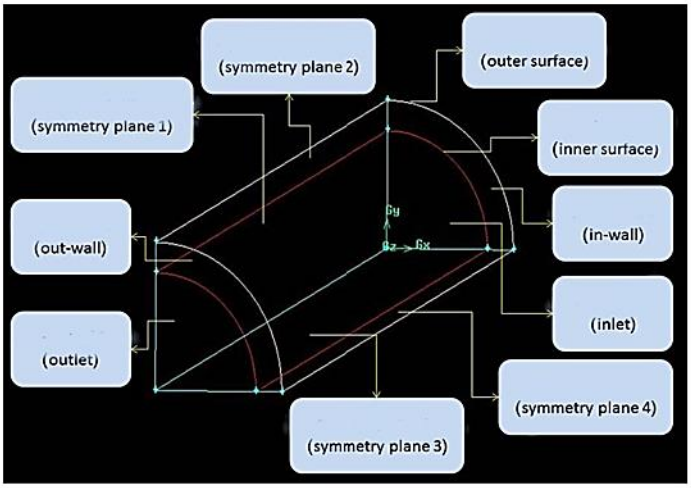

Fig. 4. Three-dimensional symmetrical geometry diagram of the circular tube.

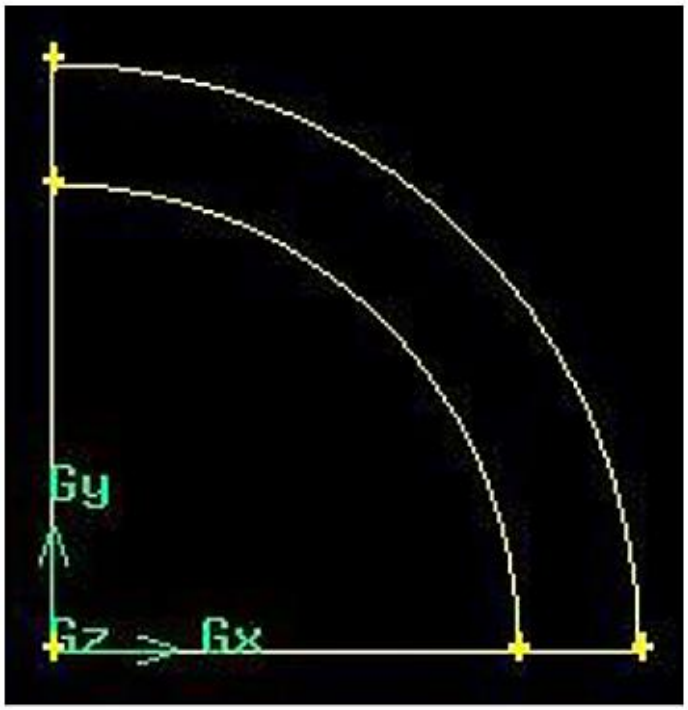

Fig. 5. Symmetrical cross-section of the circular tube.

After extending the drawn lines, the inner and outer surfaces of the tube are formed. However, the remaining faces must be created according to *Fig. 5*. As previously mentioned, the length of the tubes is 130 centimeters, with 50 centimeters at the beginning and end solely to reduce the effect of boundary conditions on the results. Only the middle section, which is 30 centimeters long, is subject to freezing conditions. Therefore, to apply the appropriate boundary condition for each part, the outer shell must be divided into three sections, which are labeled as outer shell 1, 2, and 3 in *Fig. 6*. The geometry of the circular tube is then completed by creating the internal and external volumes, which represent the fluid and the solid (tube material), respectively.

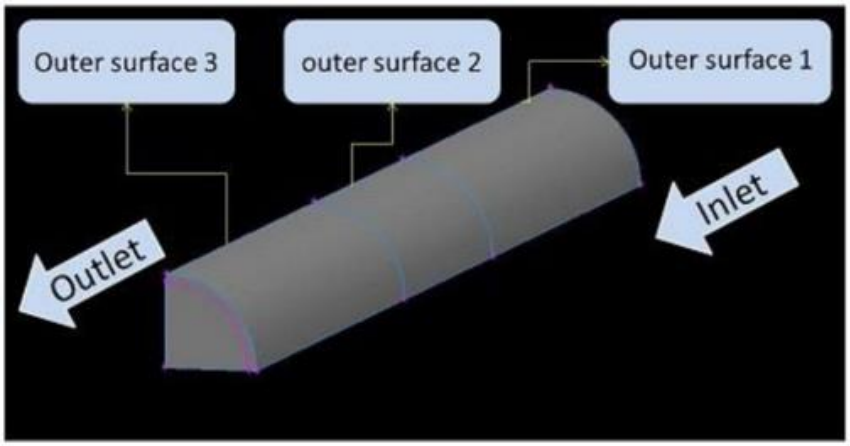

Fig. 6. Labeling of the different sections of the outer shell.

3.2 | Noncircular Tubes

The three-dimensional diagram of noncircular tubes, drawn with symmetry (one-fourth of the three-dimensional geometric shape), is shown in *Fig. 7*.

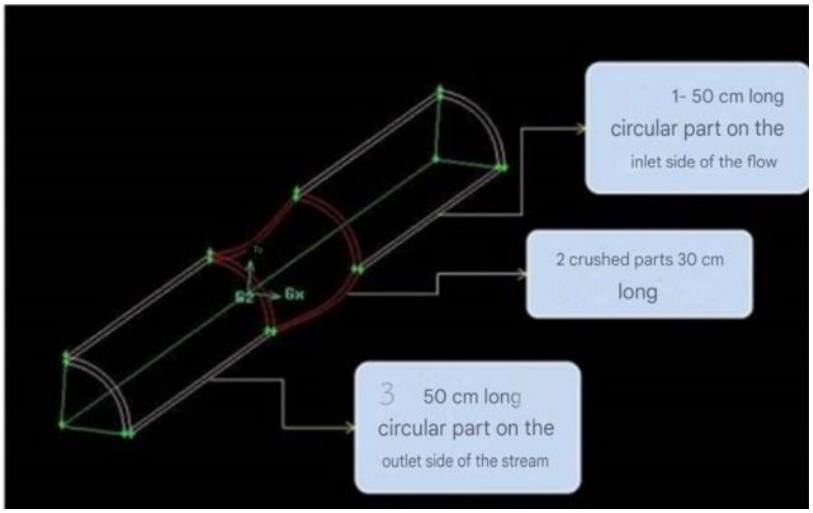

Fig. 7. Symmetrical geometry diagram of the flattened tube.

As observed, the shape of the noncircular tubes is not uniform. In the section where the tube is to be frozen under liquid nitrogen temperature, the tube is flattened, creating an irregular shape that must be accurately and realistically drawn. Therefore, initially, the section of the tube that is to be flattened is examined using one of the solid simulation software tools to determine the precise shape of the deformation. In this case, ANSYS Workbench software is used. This software offers various environments for modeling and simulating different problems in the fields of fluids and solids.

3.3 | Mesh

The next step is the meshing of the model, which is carried out using the Mapped Face Meshing option and selecting all the internal and external surfaces of the tube. The mesh size is set to 0.005 meters.

3.4 | Mesh Independence Results

In the simulation process, results for several mesh sizes were examined, and variations in key variables such as temperature and velocity were analyzed. After comparing the results, the mesh size of 0.005 meters was chosen as the optimal size, as the changes in results for finer meshes were negligible. Given that the cross-sections at the beginning and end of the tube are fixed and do not deform, the cross-sectional size varies along the tube, gradually decreasing from both ends to the center of the tube. A three-

dimensional view of the flattened tube is shown in *Fig. 8*. Excessive flattening leads to an excessive increase in flow rate and turbulence, which can negatively affect the formation of ice and the closure of the tube. Therefore, in this study, the maximum amount of flattening was considered to be up to 25% of the tube's initial diameter. The flattening amount refers to the ratio of the change in diameter to the initial diameter. The greatest deformation occurs in the middle section of the tube, and the flattening amount is calculated based on this section. *Table 2* presents specifications of the flattened tubes.

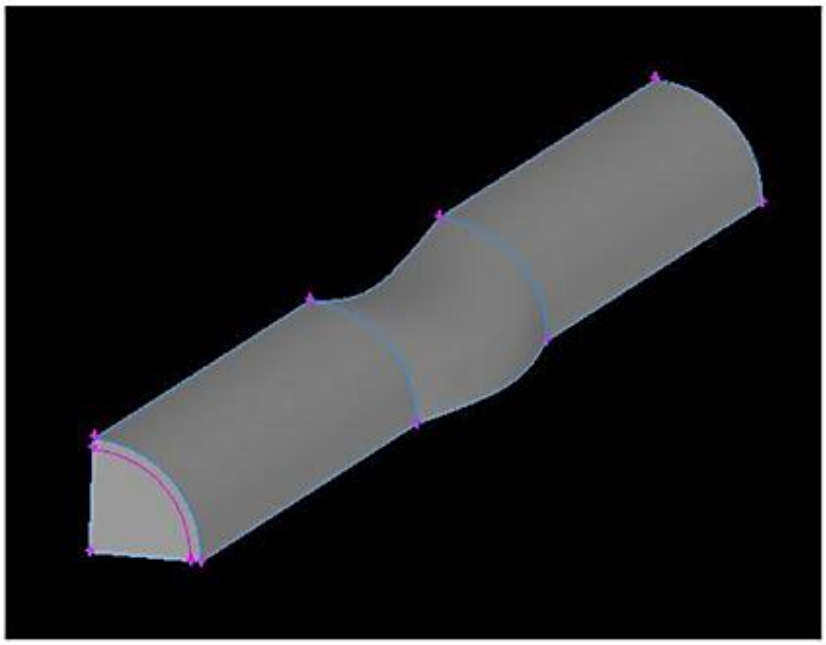

Fig. 8. Three-dimensional view of the flattened tube.

Table 2. Specifications of the flattened tubes.

Pipe Size (Inch)	of Percent Thickness Change (%)	Maximum in Change Thickness (mm)	Larger Outer Diameter (mm)	Smaller Outer Diameter (mm)	Ratio of Smaller to Larger Outer Diameter (%)
1	25	0.41	25.08	15.58	61
1	20	0.34	25.04	16.44	66
1	15	0.27	25.02	17.22	69
1	10	0.22	25.00	18.00	72
1	5	0.15	25.01	18.98	76
1	0	0.00	25.00	20.48	82
2	25	1.11	51.58	32.08	62
2	20	0.94	51.54	34.08	66
2	15	0.68	51.52	36.00	70
2	10	0.42	51.56	38.04	74
2	5	0.21	51.60	40.08	78
2	0	0.00	51.58	42.08	82
3	25	1.42	76.66	48.08	63
3	20	1.14	76.61	51.08	67
3	15	0.85	76.60	54.08	71
3	10	0.57	76.56	57.08	75
3	5	0.28	76.60	60.08	78
3	0	0.00	76.58	63.08	82

Table 2. Continued.

Pipe Size (Inch)	of Percent Thickness Change (%)	Maximum in Change Thickness (mm)	Larger Outer Diameter (mm)	Smaller Outer Diameter (mm)	Ratio of Smaller to Larger Outer Diameter (%)
4	25	1.88	102.61	64.78	63
4	20	1.51	102.53	68.08	66
4	15	1.13	102.54	71.08	69
4	10	0.75	102.56	74.08	72
4	5	0.38	102.54	77.08	75
4	0	0.00	102.53	80.08	78
5	25	2.35	127.98	81.08	63
5	20	1.88	127.94	85.08	66
5	15	1.42	127.92	89.08	70
5	10	0.95	127.93	93.08	73
5	5	0.47	127.94	97.08	76
5	0	0.00	127.92	101.08	79

The shape resulting from the flattening for each case must be drawn using Gambit software. As shown in *Fig. 9*, the final shape has a section where the middle part is flattened. To accurately draw the flattening, the sectioning method has been used. For this purpose, the cross-sectional shape located in the middle of the tube, shown in *Fig. 9. a*, and the longitudinal section of the tube, shown in *Fig. 9. b*, are sectioned using auxiliary software, and these points are drawn in Gambit. With these lines, the internal and external shells of the flattened tube can be drawn.

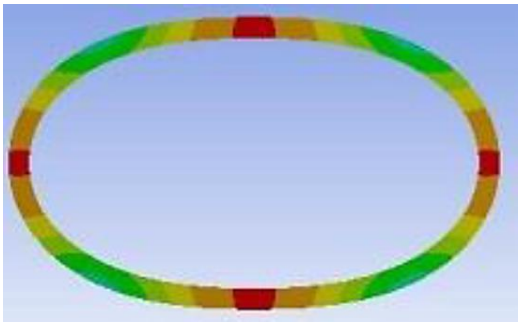

a.

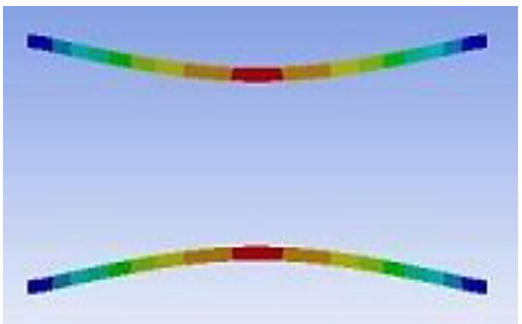

b.

Fig. 9. Longitudinal and cross-sectional views of the flattened tube; a. Cross-sectional view, and b. Longitudinal section.

As shown in *Fig. 7*, the cross-sections at the beginning and end of the flattened section remain circular and do not deform, which is due to fixing both ends of the tube. By extending each of these sections along the tube's axis, the external and internal surfaces of the entire shape are created. The remaining faces are exactly like those of the circular tube (*Fig. 7*), and with the definition of internal and external volumes, the geometric shape creation process is completed.

3.6 | Boundary Condition

As explained in the modeling section, there are various types of boundary conditions that are applied according to the specific problem. *Table 3* lists the boundary conditions used in the modeling of pipe freezing, which must have their appropriate values determined in the simulation section. To determine the boundary values, the assumptions of the problem must be clearly defined. In this study, the freezing time for both circular and flattened tubes is examined under the following assumptions:

I. Water is used as the fluid.

II. The initial fluid temperature is assumed to be 20°C.

III. The problem is solved for tubes with sizes ranging from 1 to 5 inches.

If the temperature and pressure of the fluid entering the boundary are known, the inlet pressure condition can be applied for that. The pressure difference that creates flow in the pipeline can be calculated using *Eq. (16)*.

Table 3. Boundary conditions.

Surface Name	Boundary Condition Type
Inlet	Pressure-inlet
Outlet	Pressure-inlet
Inwall	Wall
Outwall	Wall
Inner surface	Wall
Outer surfaces	Wall
XZ planes	Symmetry
YZ planes	Symmetry

$$P = \rho\left(f\frac{L}{d}\frac{V^2}{2}\right), \tag{16}$$

where P is the pressure in Pascals (Pa), ϱ is the fluid density in kg/m³, f is the friction factor, d is the inner diameter of the tube in meters (m), V is the flow velocity in meters per second (m/s), and L is the length of the tube in meters (m).

To use *Eq. (16)*, the friction factor must be specified. For laminar flow, this value can be obtained from relation *Eq. (17)*, while for turbulent flow, it is derived from various available relations and can be determined using the Moody chart.

$$f = \frac{64}{Re}. \tag{17}$$

In this relation, Re represents the Reynolds number, which has specific values depending on the flow conditions: laminar, transitional, or turbulent. In general, the flow regime is determined by the corresponding Reynolds number, where for laminar flow in a pipe, the Reynolds number is considered to be less than 2000.

4 | Result and Discussion

This study uses the method of CFD to simulate the freezing time in circular and flattened tubes with initially at 20°C water for the following conditions:

I. Circular pipes (1 to 4 inches) with no flow.

II. Circular pipes (1 and 2 inches) with flow, at four different velocities in the laminar flow regime.

III. Flattened pipes (1 to 4 inches) with degrees of flattening, no flow.

IV. Flattened pipes (1 and 2 inches) with flow, subjected to different flattening levels and four different velocities in the laminar flow regime.

Table 4 displays the freezing time for all the cases under study. Both 1-inch and 2-inch pipe velocity columns contain the same values because the velocities of 10, 20, 30, and 40 mm/s fall in the laminar flow regime for both pipe diameters. For the 3-inch pipe, though, lower velocity values were selected to maintain the flow as laminar.

The column of pressure difference provides the pressure that must be supplied in order to achieve the specified velocity, which is the outlet and inlet pressure difference of the pipe. These were calculated from Bernoulli's equation.

The columns beneath the circular and flattened pipes, corresponding to five various degrees of flattening, indicate the freezing time in minutes for each case.

Table 4. Freezing time of 20°C water at different velocities in circular and deformed pipes.

Pipe Size (Inch)	Speed (mm/s)	Pressure Difference (Pa)	Freezing Time (Min)					
			Circular	5%	10%	15%	20%	25%
1	0	0	3.33	3.25	3.08	2.92	2.67	2.17
	10	0.705	3.67	3.58	3.5	3.33	3.17	2.83
	20	1.41	4.08	4	3.83	3.67	3.5	3.25
	30	2.11	4.518	4.42	4.25	4.17	3.92	3.67
	40	2.82	5.17	5	4.83	4.67	4.42	4
2	0	0	13	11	10.5	10	9.5	9
	10	0.172	14.5	13.5	13	12	11.5	10
	20	0.3427	16	14.5	14	13	12.5	12
	30	0.517	21	17.5	17	15.5	15	14
	40	0.69	23	21	20	19.5	18.5	17
3	0	0	29	27	26	25	24	23
	5	0.034	39	38	37	36	34	32
	10	0.069	42	41	40	39	37	36
	15	0.103	55	52	50	47.5	46	44
	20	0.136	58	56	55	54	52	50
4	0	0	48	47	46	45	43.5	42

As *Table 4* shows, it can be seen that freezing time in flattened pipes is less than that in circular pipes. Furthermore, the greater flattening, the less the freezing time. Additionally, the influence of flattening on freezing time is more for larger-diameter pipes. In conclusion, flattening in larger-diameter pipes produces a larger percentage decrease in freezing time.

By comparing freezing time at varying velocities for the same pipe diameter, and comparing freezing time among various diameters at the same velocity, it is evident that pipe diameter influences freezing time more than velocity. Yet, by comparing freezing time in a constant diameter, it is evident that doubling the velocity will not always double the freezing time within the velocity range being investigated.

Thus, it can be concluded that the influence of pipe diameter on freezing time is far more pronounced than that of fluid velocity.

4.1|Freezing Time Charts Based on Pipe Diameter

The freezing time for a stationary fluid (zero velocity) in pipe diameters ranging from 1 to 4 inches is depicted in *Fig. 10*, whereas *Fig. 11* presents the freezing times at flow velocities of 10 and 20 mm/s for pipe diameters between 1 and 3 inches. For the 4-inch pipe, the freezing times at flow velocities of 10 and 20 mm/s are more

than one hour. Since the simulation time was limited to a maximum of one hour, these situations are beyond the designated time frame and thus have been excluded from the results.

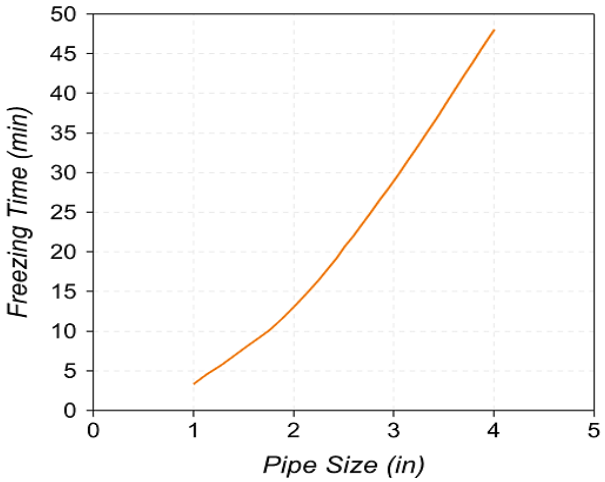

Fig. 10. Freezing time vs. diameter in stationary circular pipes (1 to 4 inches, no flow).

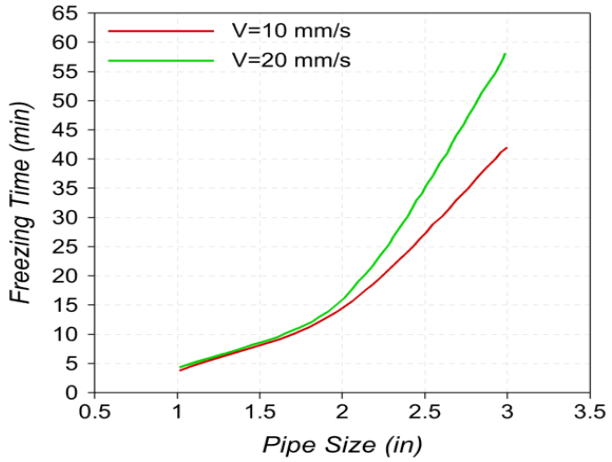

Fig. 11. Freezing time vs. diameter in circular pipes (1, 2, and 3 inches) for flow velocities of 10 and 20 mm/s.

The data presented in *Fig. 10* reveal that, for a stationary fluid, freezing time and pipe diameter bear a nonlinear and upward curve correlation. Freezing time comparison based on various pipe sizes reveals that, with each one-unit increase in pipe size, there is a corresponding increase of 5 units in freezing time. Thus, the freezing time of a 5-inch pipe will increase by 25 units from that of a 4-inch pipe, which is approximately 70 minutes. The curves in *Fig. 11*, which pertain to pipes with fluid flow, have a steeper slope than the respective curves of stationary pipes.

It shows that the rise in freezing time is higher in flowing pipes compared to stationary pipes. Comparison between the 10 mm/s and 20 mm/s velocity curves reveals that an increase in velocity corresponds to a freezing time curve that is more steeply inclined. The trend in the 20 mm/s curve, as opposed to the 10 mm/s curve, is that at much higher velocities, the slope of the curve may tend to infinity, hence creating a vertical asymptote in the graphical representation.

In other words, at high speeds, freezing time is seemingly approaching infinity, which can only mean the pipe would never freeze at all. Another, and perhaps a more interesting note, is how closely the two graphs in *Fig. 11* track for pipe diameters of less than 2 inches. It will mean that the influence of elevated velocity on freezing time is lower in smaller pipes than it would be in bigger pipes. It is due to the Reynolds number of flow dynamics. The Reynolds number at lower velocities is close to the transitional regime for wide-diameter pipes.

Consequently, when the velocity increases proportionally for different pipe diameters, flow behavior in larger pipes and smaller pipes has a varying influence on freezing and ice layer growth.

4.2 | Freezing Time Charts Based on Pipe Diameter

Fig. 12 is for the 1-inch pipe, *Fig. 13* for the 2-inch pipe, and *Fig. 14* for the 3-inch pipe. In all three charts, as we would anticipate, an increase in velocity results in an increase in freezing time, with the topmost curve being the circular pipe.

In *Fig. 12*, the plotted lines have nearly the same slope, meaning that in the 1-inch pipe, the influence of velocity on freezing time is roughly the same for both circular and flattened pipes with varying degrees of deformation.

Similarly, in *Figs. 13* and *14*, the curves for different flattening levels remain close to each other, but the slope of the circular pipe curve is steeper than that of the flattened pipes. A general trend can be identified for the three freezing time charts vs. velocity: the difference in slopes between circular and flattened pipes becomes larger with pipe diameter. It indicates that the influence of flattening in minimizing freezing time is more dominant at larger pipe diameters.

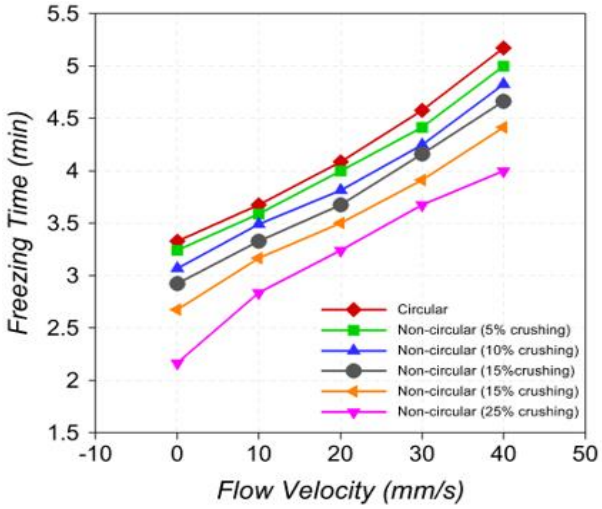

Fig. 12. Freezing time vs. fluid velocity in a 1-inch pipe.

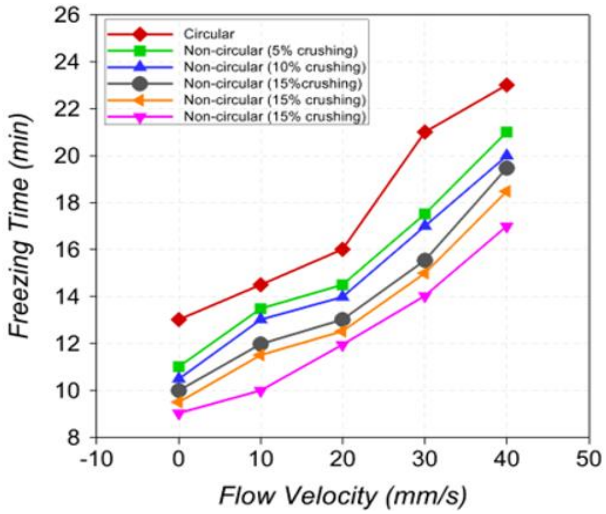

Fig. 13. Freezing time vs. fluid velocity in a 2-inch pipe.

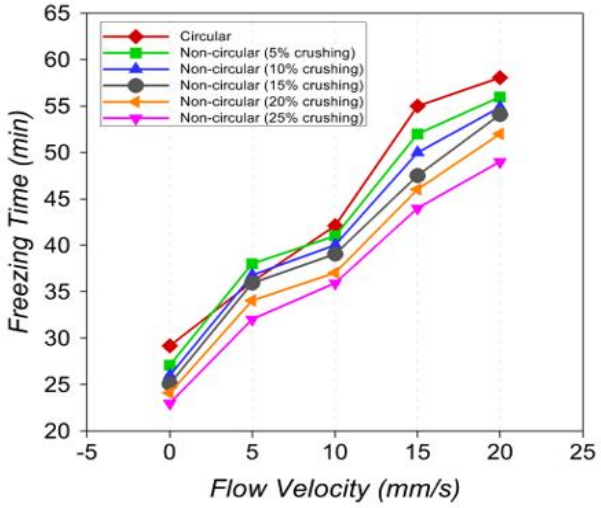

Fig. 14. Freezing time vs. fluid velocity in a 3-inch pipe.

4.3 | Freezing Time Charts Based on Pipe Diameter

To compare the circular and flattened pipes of every diameter, all cases are plotted in the same coordinate system. For the flattening level-based freezing time graph, the circular pipe is assigned a flattening value of 0%. The plots of freezing times as a function of degree of flattening at varying velocities are provided in *Fig. 15* for the 1-inch pipe, *Fig. 16* for the 2-inch pipe, and *Fig. 17* for the 3-inch pipe.

Each of the three preceding charts shows a trend with decreasing values, and it can be inferred that the greater degree of flattening results in lower freezing time. In the graph of the 1-inch pipe, the lines are almost parallel, while in the graphs of the 2-inch and 3-inch pipes, there is a steeper drop. It indicates that the greatest changes take place in pipes with flow. That is, for pipes with no flow, the rate of reduction in freezing time is almost constant.

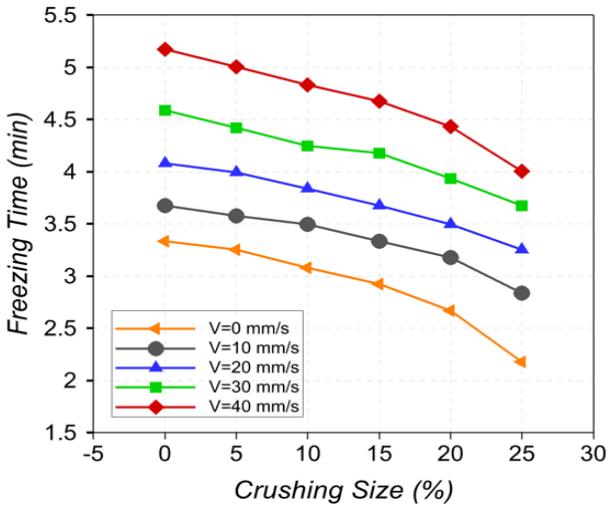

Fig. 15. Freezing time vs. deformation size at different velocities in a 1-inch pipe.

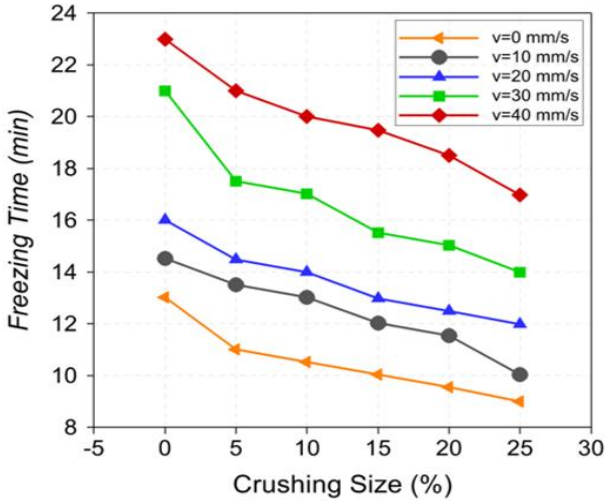

Fig. 16. Freezing time vs. deformation size at different velocities in a 2-inch pipe.

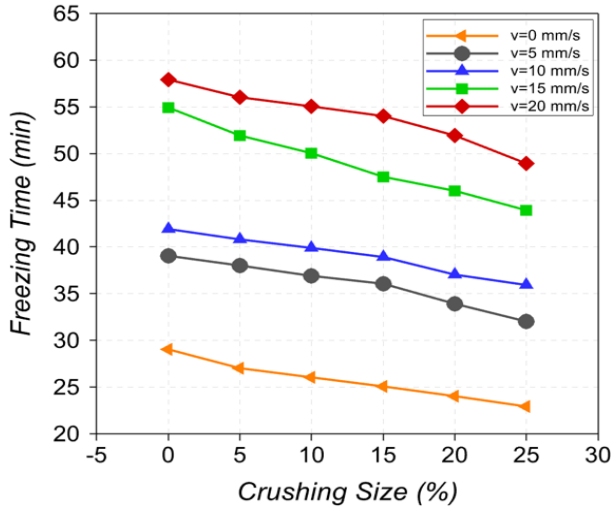

Fig. 17. Freezing time vs. deformation size at different velocities in a 3-inch pipe.

4.4 | Simulation Results

Figs. 18 and *19* are the fluid temperature profile and freezing boundary at 1260 seconds, midway of a 2-inch circular pipe at a velocity of 30 mm/s.

Similarly, *Figs. 20* and *21* illustrate the fluid temperature distribution and freezing boundary at 1020 seconds in the midsection of a 2-inch diameter circular pipe at a flow rate of 40 mm/s.

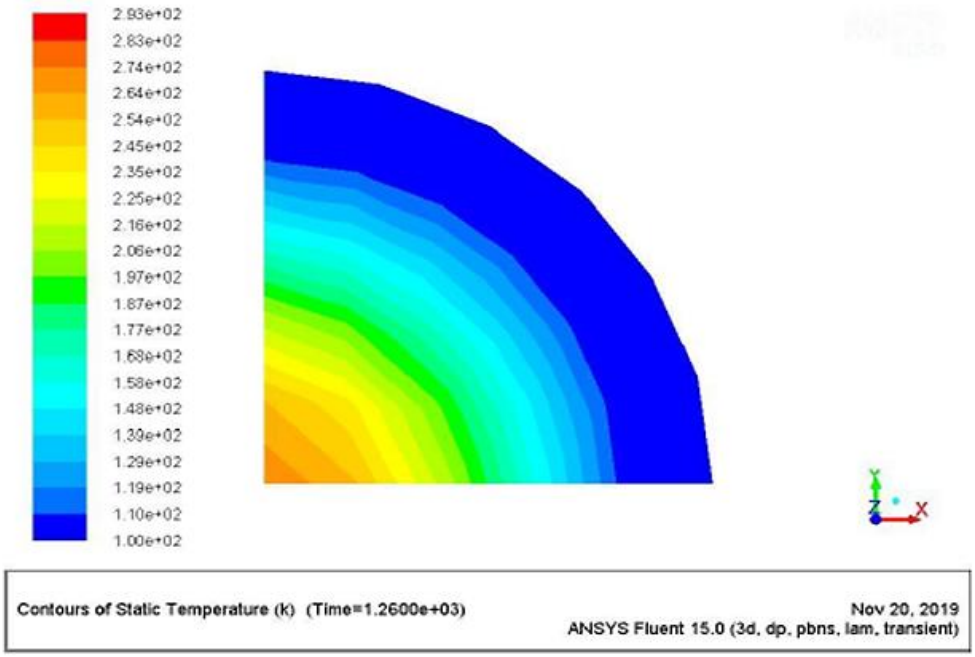

Fig. 18. Fluid temperature contour in the cross-section of a 2-inch circular pipe at the midpoint of the refrigerant zone (after 1260 seconds).

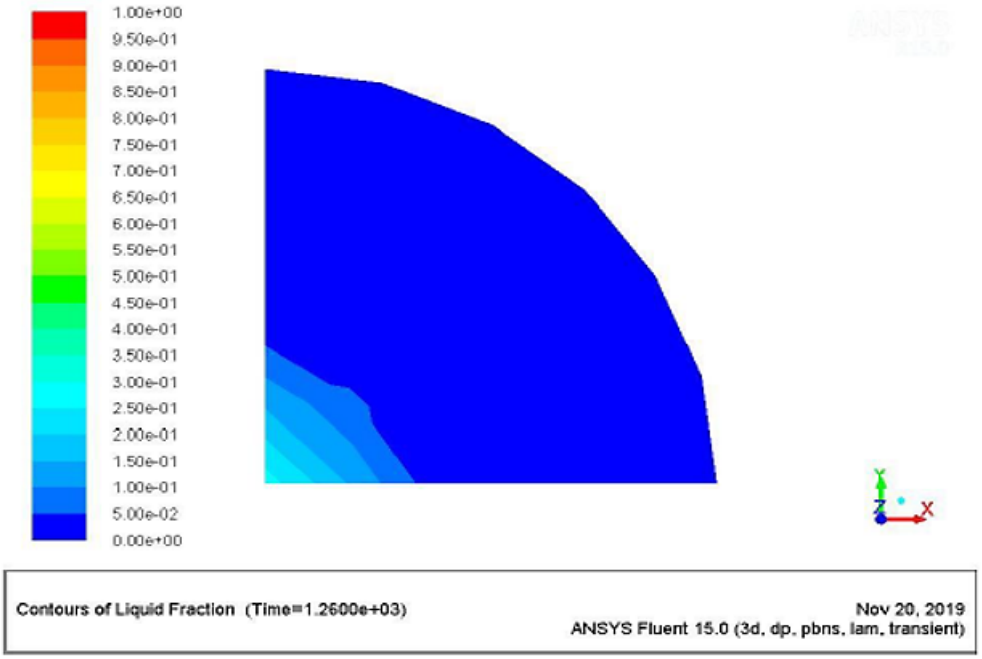

Fig. 19. Freezing boundary contour in the cross-section of a 2-inch circular pipe at the midpoint of the refrigerant zone (after 1260 seconds).

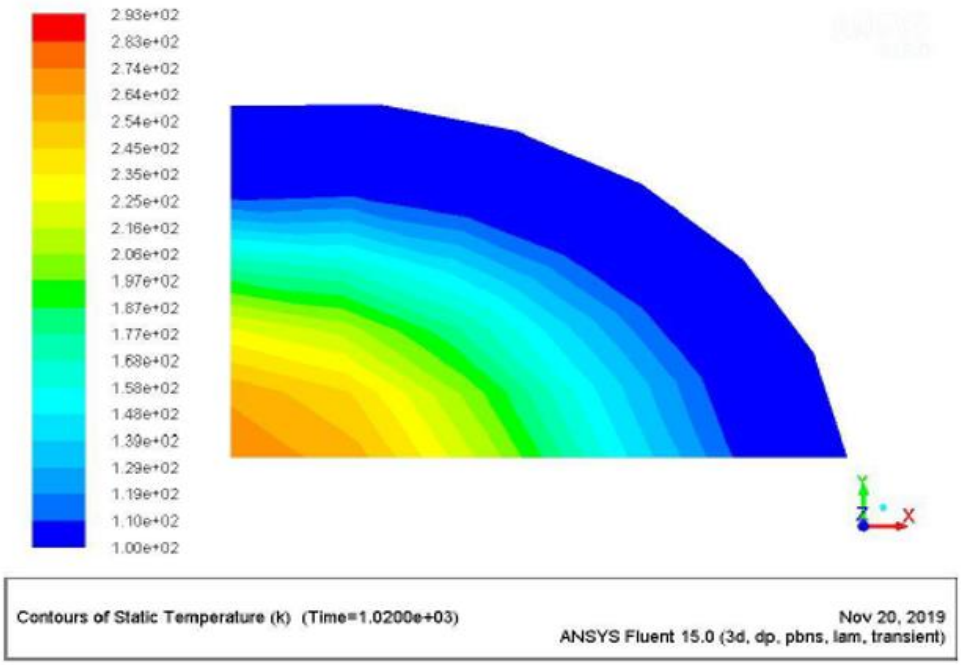

Fig. 20. Fluid temperature contour in the cross-section of a 2-inch pipe with 25% deformation at the midpoint of the refrigerant zone (after 1020 seconds).

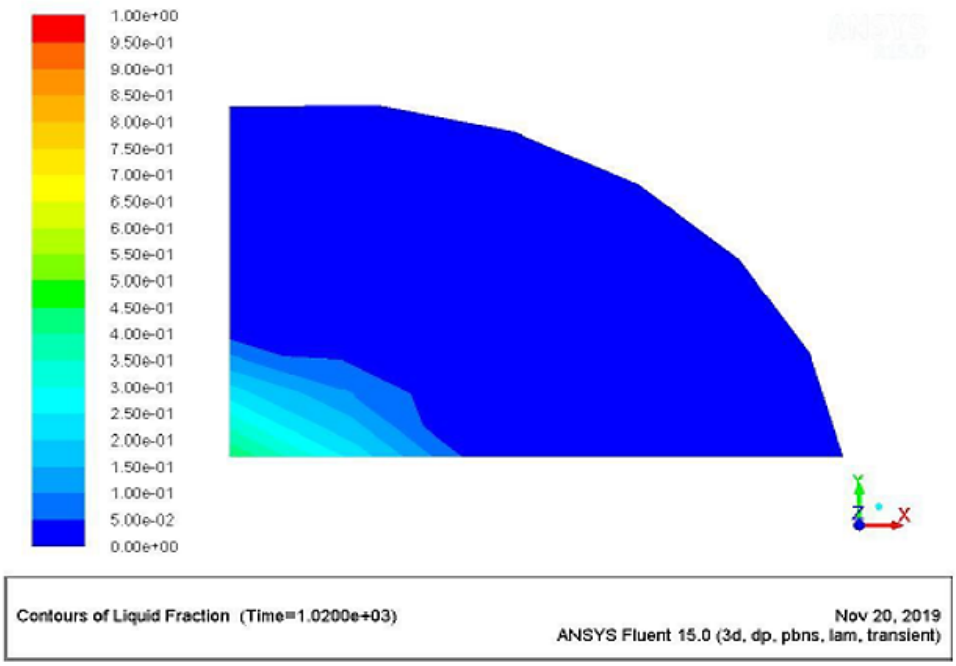

Fig. 21. Freezing boundary contour in the cross-section of a 2-inch pipe with 25% deformation at the midpoint of the refrigerant zone (after 1020 seconds).

The purpose of presenting *Figs. 18-21* show the thermal distribution and freezing front at the end of the simulation. Both circular and flattened pipes' figures are presented to allow comparison and complement the overall assessment.

The freezing boundary contour values vary from 0 to 1, with 0 indicating complete freezing and 1 indicating the entirely liquid phase. (Completely frozen and completely liquid are about the state of the fluid.) Thus, by examining the contours of the freezing boundary, one can say if the cross-section shown is entirely frozen.

5 | Conclusion

This study investigated the influence of pipe geometry and flow conditions on the freezing process in fluid transmission pipelines using CFD simulations. The findings confirmed that pipe diameter, fluid velocity, and especially pipe deformation significantly affect freezing time and the formation of stable ice plugs. Flattened pipes exhibited reduced freezing times compared to circular ones, with the greatest reductions observed in larger diameter pipes and higher levels of flattening. The results also showed that while increased fluid velocity leads to longer freezing times, the effect is more pronounced in larger pipes. Furthermore, the freezing time increases non-linearly with pipe diameter, and there is a critical velocity threshold beyond which freezing becomes ineffective. The visualization of temperature distribution and freezing front in both circular and deformed pipes validated the simulation outcomes. These insights can be effectively used to optimize pipeline maintenance operations by reducing fluid loss, minimizing system downtime, and improving safety and environmental outcomes—particularly in industries like power generation, oil and gas, and chemical processing.

Authors' Contributions

All aspects of the research and manuscript preparation were carried out by the author. The author has read and approved the final version of the manuscript.

Funding

This study did not receive any specific funding from public, commercial, or non-profit funding agencies.

Data Availability

All data are included in the text.

Conflict of Interest

The author declares that he does not have any conflict of interest.

Consent for Publication

The author has given consent for the publication of this manuscript.

Ethics Approval and Consent to Participate

This study does not involve any research conducted on human participants or animals.

References

[1] Kia, S., Khanmohammadi, S., & Jahangiri, A. (2023). Experimental and numerical investigation on heat transfer and pressure drop of SiO2 and Al2O3 oil-based nanofluid characteristics through the different helical tubes under constant heat fluxes. *International Journal of Thermal Sciences*, *185*, 108082. https://doi.org/10.1016/j.ijthermalsci.2022.108082

[2] Kia, S. M., Nejati Jahromi, M., & Isvand, H. (2022). Numerical and experimental evaluation and processing of unsteady flow around rotating cylindrical models with three orthogonal plates under forced rotation. *Modares Mechanical Engineering*, *22*(11), 637-646. (**In Persian**). https://doi.org/10.52547/mme.22.11.637

[3] Ashrafi, N., & Sadeghi, A. (2018). Numerical simulation of visco-plastic fluid flow between two parallel plates with triangular obstacles. *Bulletin of the American Physical Society*, *63*. https://meetings.aps.org/Meeting/DFD18/Event/334178

[4] Kia, S. M., & Talebi, F. (2018). Numerical investigation of unsteady flow around a circular cylinderat different reynolds number. *The 26th Annual International Conference of the Iranian Society of Mechanical Engineers*. Semnan, Iran. Civilica. (**In Persian**). https://civilica.com/doc/1134380

[5] Kia, S. M., Nobakhti, M. H., & Khayat, M. (2020). Experimental investigation on heat transfer and pressure drop of Al2O3-base oil nanofluid in a helically coiled tube and effect of turbulator on the thermal performance of shell and tube heat exchanger. *Journal of Energy Conversion*, *7*(3), 61–80. (**In Persian**). https://dor.isc.ac/dor/20.1001.1.20089813.1399.7.3.5.6

[6] Keary, A. C., & Bowen, R. J. (1998). Analytical study of the effect of natural convection on cryogenic pipe freezing. *International Journal of Heat and Mass Transfer, 41*(10), 1129-1138. https://doi.org/10.1016/S0017-9310(97)00269-X

[7] Sparrow, E. M., Larson, E. D., & Ramsey, J. W. (1981). Freezing on a finned tube for either conduction-controlled or natural-convection-controlled heat transfer. *International Journal of Heat and Mass Transfer, 24*(2), 273-284. https://doi.org/10.1016/0017-9310(81)90035-1

[8] Keary, A. C., Syngellakis, S., & Bowen, R. J. (2001). Experimental and analytical study of thermal stresses during pipe freezing. *Proceedings of the Institution of Mechanical Engineers, Part E: Journal of Process Mechanical Engineering, 215*(1), 63-77. https://doi.org/10.1243/0954408011530307

[9] Jeong, G. H., Ahn, B. J., Seong, Y. S., & Kim, K. S. (2002). Numerical analysis of phase change and natural convection phenomena during pipe freezing process. *Proceedings of the ASME Pressure Vessels and Piping Conference (Paper No. PVP2002-1584) (pp. 145-149).* American Society of Mechanical Engineers. https://doi.org/10.1115/PVP2002-1584

[10] Alexiades, V. (2018). *Mathematical modeling of melting and freezing processes*. Routledge. https://doi.org/10.1201/9780203749449

[11] Alzoubi, M. A., Xu, M., Hassani, F. P., Poncet, S., & Sasmito, A. P. (2020). Artificial ground freezing: A review of thermal and hydraulic aspects. *Tunnelling and Underground Space Technology, 104*, 103534. https://doi.org/10.1016/j.tust.2020.103534

[12] Alzoubi, M. A., Nie Rouquette, A., & Sasmito, A. P. (2018). Conjugate heat transfer in artificial ground freezing using enthalpy-porosity method: Experiments and model validation. *International Journal of Heat and Mass Transfer, 126*, 740-752. https://doi.org/10.1016/j.ijheatmasstransfer.2018.05.059

[13] Huang, S., Guo, Y., Liu, Y., Ke, L., & Liu, G. (2018). Study on the influence of water flow on temperature around freeze pipes and its distribution optimization during artificial ground freezing. *Applied Thermal Engineering, 135,* 435-445. https://doi.org/10.1016/j.applthermaleng.2018.02.090

[14] Vitel, M., Rouabhi, A., Tijani, M., & Guérin, F. (2015). Modeling heat transfer between a freeze pipe and the surrounding ground during artificial ground freezing activities. *Computers and Geotechnics, 63*, 99-111. https://doi.org/10.1016/j.compgeo.2014.08.004

[15] Hu, M., Zhang, W., Xu, K., Yang, Z., Wang, L., Feng, Y., & Chen, H. (2024). Formation rate and energy efficiency of ice plug in pipelines driven by the cascade utilization of cold energy. *Energies, 17*(9), 1994. https://doi.org/10.3390/en17091994

[16] Mikhailenko, S. A., Buonomo, B., Manca, O., & Sheremet, M. A. (2021). Cooling of periodically heat-generated element under the convective-radiative heat transfer in a rotating domain with a thermally conducting base plate. *International Journal of Thermal Sciences, 170*, 107150. https://doi.org/10.1016/j.ijthermalsci.2021.107150

[17] Jain, A., Miglani, A., Huang, Y., Weibel, J. A., & Garimella, S. V. (2019). Ice formation modes during flow freezing in a small cylindrical channel. *International Journal of Heat and Mass Transfer, 128*, 836-848. https://doi.org/10.1016/j.ijheatmasstransfer.2018.08.051

[18] Gilpin, R. R. (1981). Ice formation in a pipe containing flows in the transition and turbulent regimes. *Journal of Heat Transfer, 103*(2), 363–368. https://doi.org/10.1115/1.3244467

[19] Liu, F L., Fan, S. K. S., Ndi, E., & Tu, J. F. (2021). An efficient no-shutdown pipe-fixing freezing design for water management system in hospitals during COVID-19: A case study. *Water*, *13*(19), 2725. https://doi.org/10.3390/w13192725

[20] Bijan Fard, S. H., & Karimi, A. (2005). Design and manufacture of pipeline freezing device. *The Fourth Conference on Fuel Consumption Optimization in Buildings*. Tehran, Iran, Civilica. (**In Persian**). https://civilica.com/doc/2694

[21] Park, Y. D., Cho, H. C., Choi, B. I., & Kim, K. S. (2001). An experimental study for the liquid freezing phenomena in a pipe during ice plugging. *Transactions of the Korean Society of Mechanical Engineers. b*, *25*. (**In Korean**). https://doi.org/10.22634/KSME-B.2001.25.3.366

[22] Burton, M. J. (1986). *An experimental and numerical study of plug formation in vertical pipes during cryogenic pipe freezing* [Thesis]. https://eprints.soton.ac.uk/460752/

[23] Tavner, A. C. R. (1992). *An experimental study of ice formation and convection during cryogenic pipe freezing* [Thesis]. https://eprints.soton.ac.uk/461013/

[24] Bowen, R. (2000). *An experimental study of ice formation in pipes* [Thesis]. https://www.researchgate.net/publication/361920351